Supplementary Materials

Privacy-preserving gait biometrics via synchronous mechanical and bioelectrical co-sensing and ciphertext-domain inference

Yexi Jin[1], Ruolin Wang[2], Jianyu Lin[1], Yu Lu[1], Jing Zhang[1], Xingwen Zhou[1], Baijie Cheng[2,*], Liguo Chen[1,*]

[1]School of Mechanical and Electrical Engineering, Soochow University, Suzhou 215000, Jiangsu, China.
[2]College of Chemistry and Chemical Engineering, Donghua University, Shanghai 201620, China.

[*]**Correspondence to:** Dr. Baijie Cheng, College of Chemistry and Chemical Engineering, Donghua University, Shanghai 201620, China. E-mail: 1222004@mail.dhu.edu.cn; Prof. Liguo Chen, School of Mechanical and Electrical Engineering, Soochow University, Suzhou 215000, Jiangsu, China. E-mail: chenliguo@suda.edu.cn

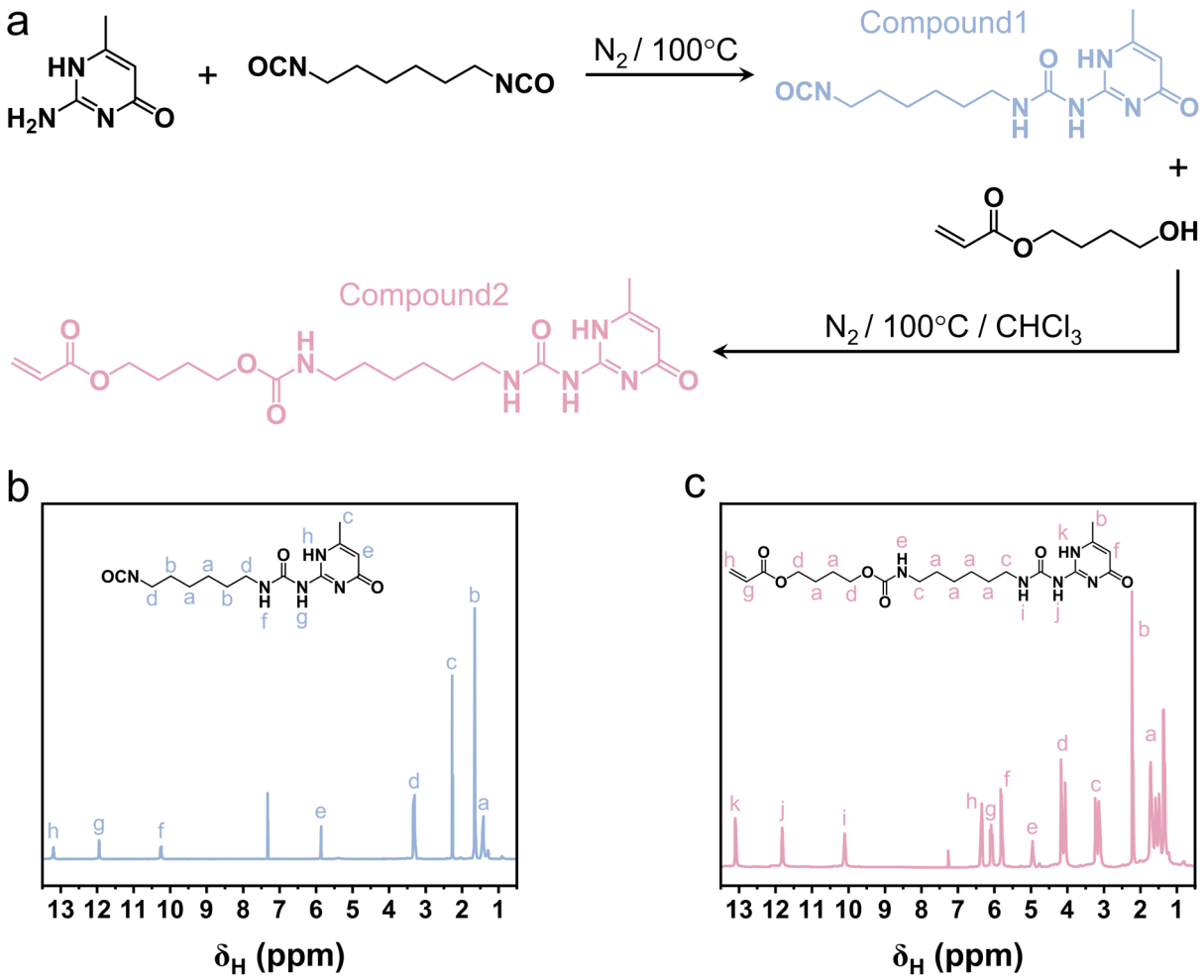

Supplementary Figure 1. a) Synthetic route of compound1 (UPy-NCO) and compound2 (UPy-HBA). b) ^{1}H NMR spectrum of UPy-NCO recorded at 298 K in $CDCl_3$. c) ^{1}H NMR spectrum of UPy-HBA recorded at 298 K in $CDCl_3$.

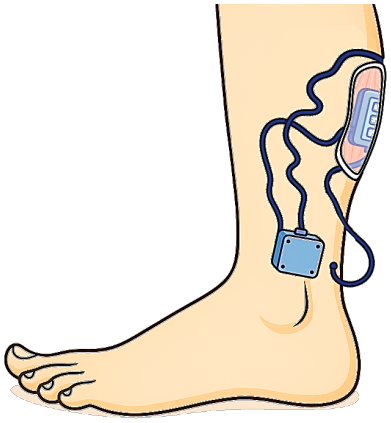

Supplementary Figure 2. Wearing illustration of the multimodal identity recognition device.

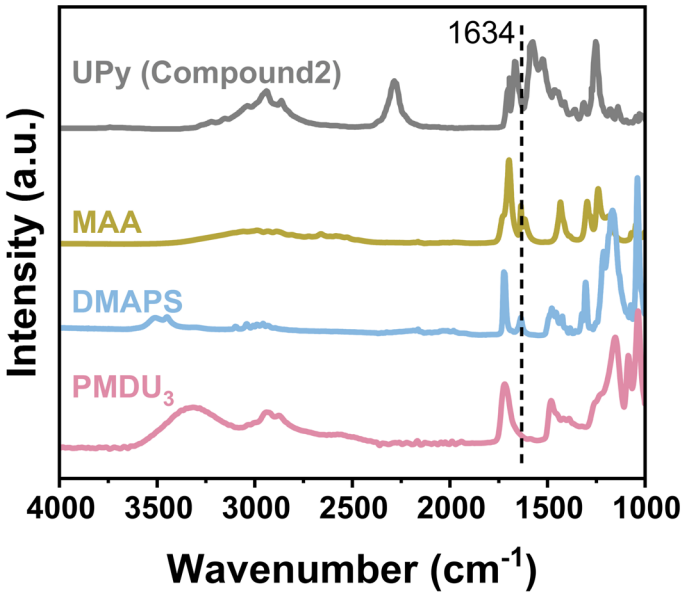

Supplementary Figure 3. FT-IR spectra of the $PMDU_3$ eutectogel and its raw monomers at 25 °C.

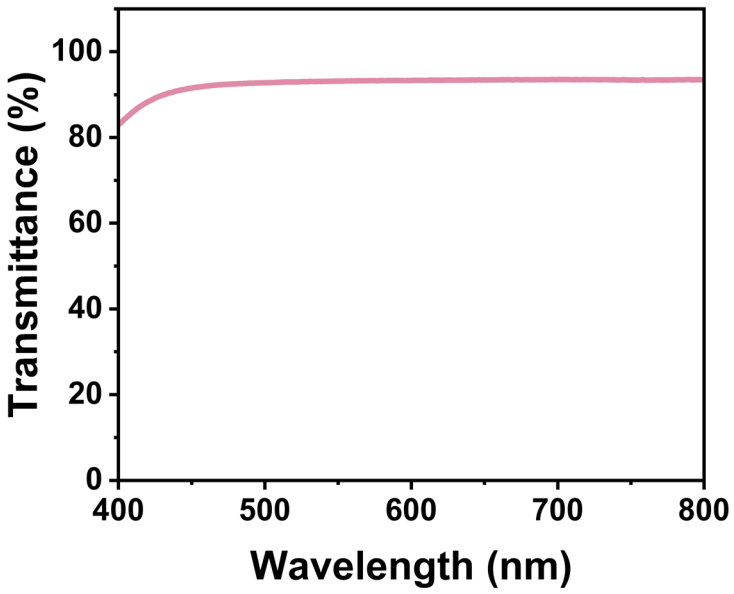

Supplementary Figure 4. Visible transmittance spectra of $PMDU_3$ eutectogel.

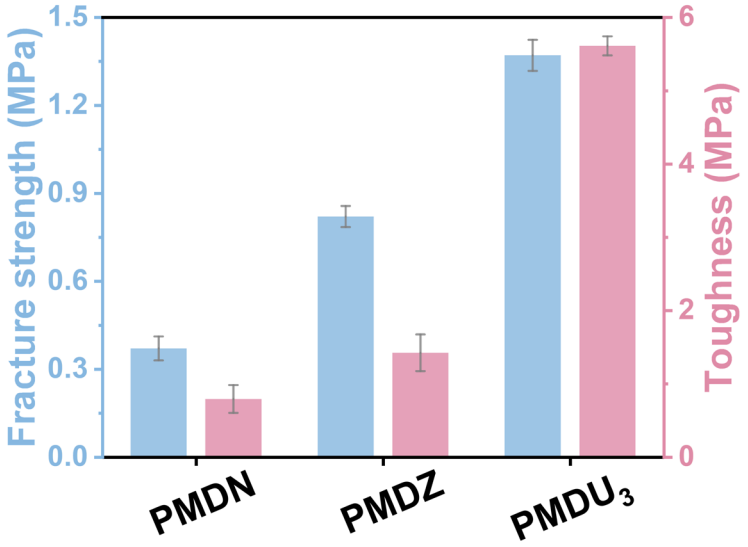

Supplementary Figure 5. Fracture strength and toughness of PMDN, PDMZ, and $PMDU_3$ eutectogels.

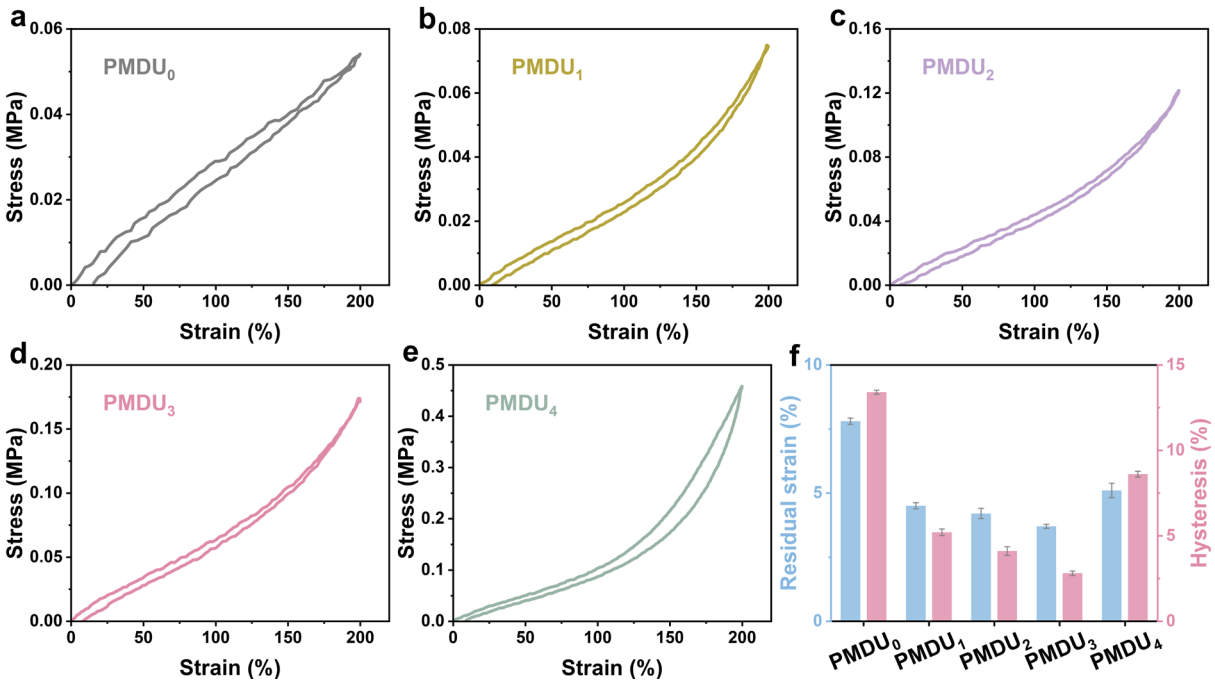

Supplementary Figure 6. a-e) Cyclie tensile testing curves of $PMDU_{0\text{-}4}$ at a strain of 200%. f) Corresponding hysteresis ratio and residual strain.

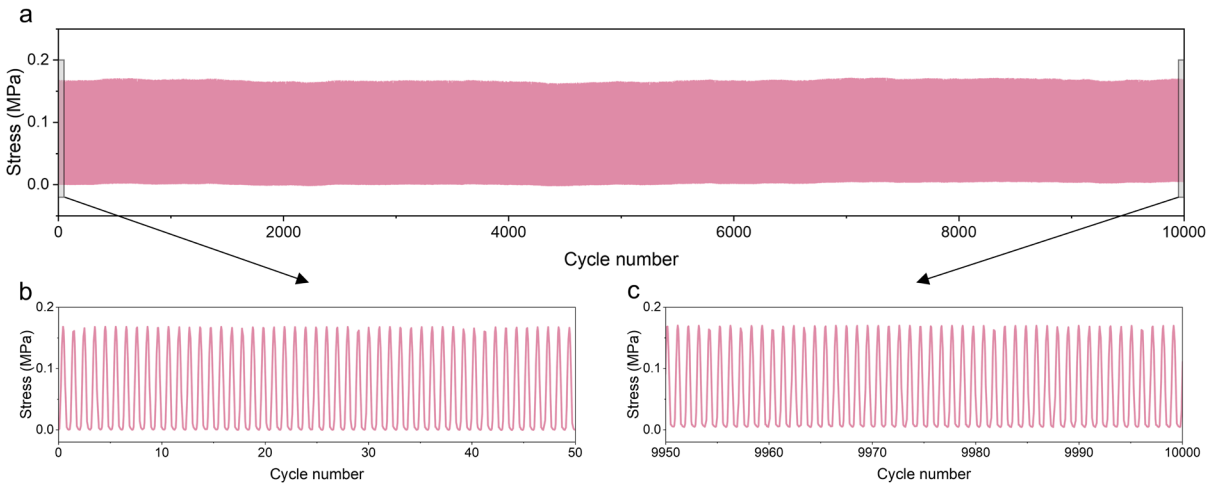

Supplementary Figure 7. a) Stress variation of the $PMDU_3$ eutectogel during 10,000 loading-unloading cycles. b) Local magnified view of the 1st to 50th cycles. c) Local magnified view of the 9950th to 10000th cycles.

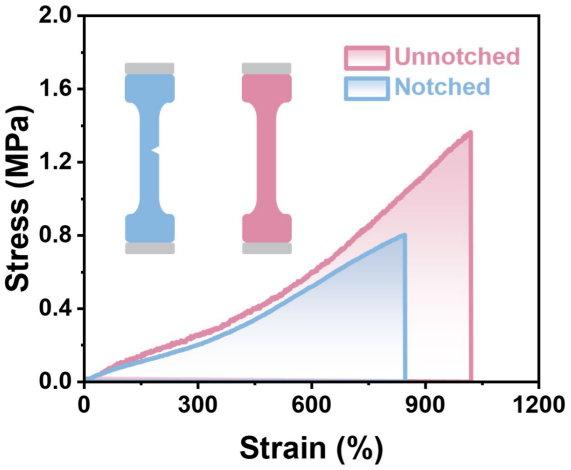

Supplementary Figure 8. Tensile stress-strain curves of notched and unnotched $PMDU_3$ eutectogel.

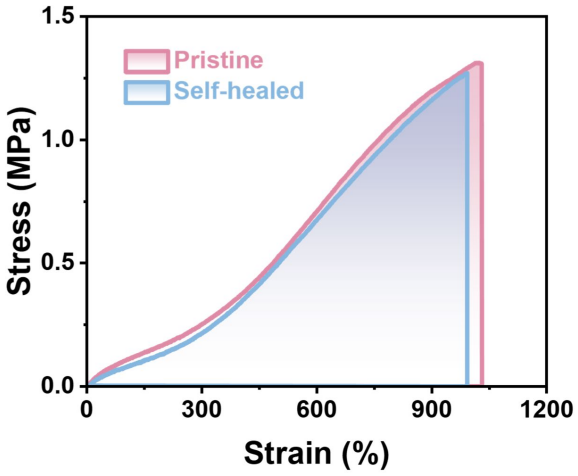

Supplementary Figure 9. Tensile stress-strain curves of self-healed and pristine $PMDU_3$ eutectogel.

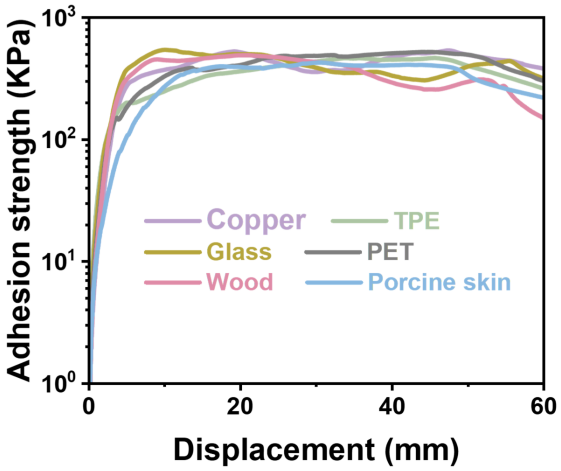

Supplementary Figure 10. 90° peeling curves and corresponding interfacial toughness of the $PMDU_3$ eutectogel with various substrates.

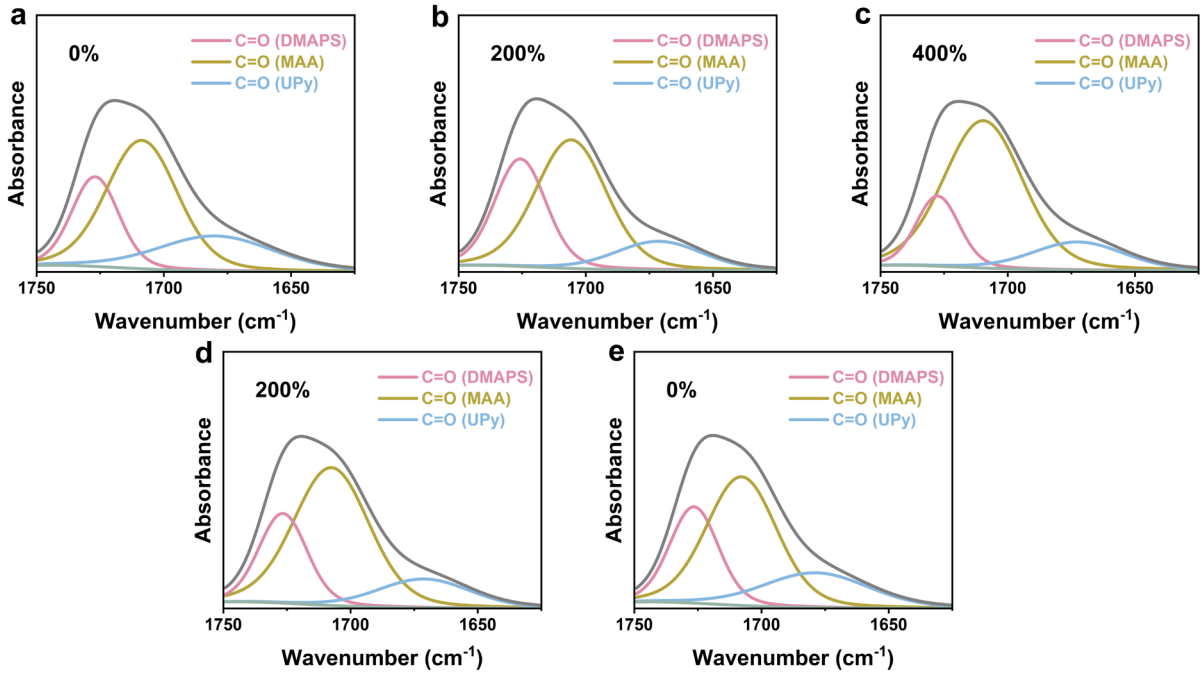

Supplementary Figure 11. In situ curve-fitted infrared spectra of the $PMDU_3$ eutectogel in the ν(C=O) region during tensile testing. The ν(C=O) peak was fitted using three dominant species. a) Original state. b) Tensile strain = 100%. c) Tensile strain = 200%. d) Tensile strain recovered to 100%. e) Tensile strain recovered to 0.

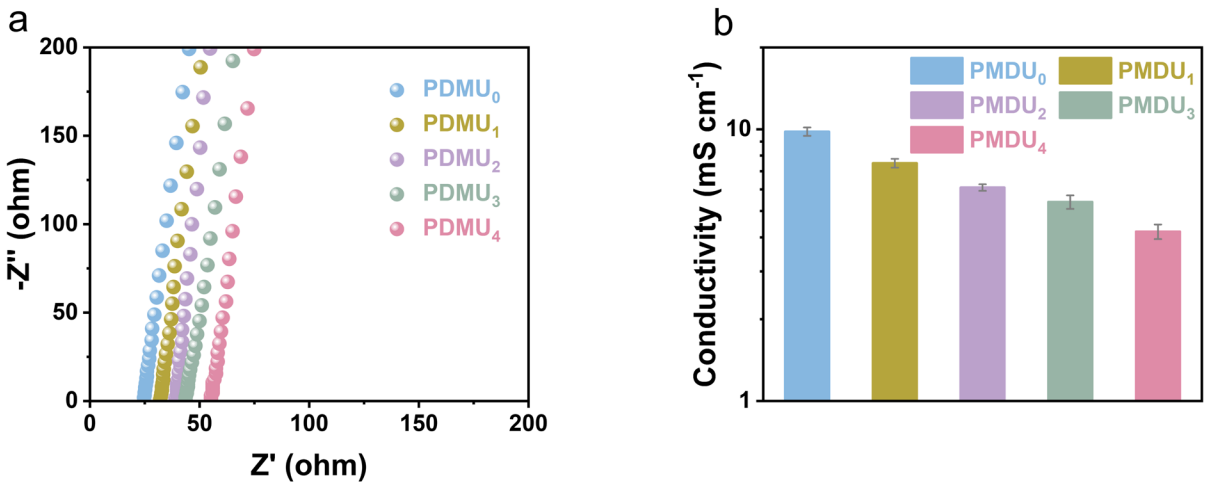

Supplementary Figure 12. a) Electrochemical impedance spectroscopy (EIS) of $PMDU_{0\text{-}4}$ eutectogels. b) Ionic conductivity of $PMDU_{0\text{-}4}$ eutectogels.

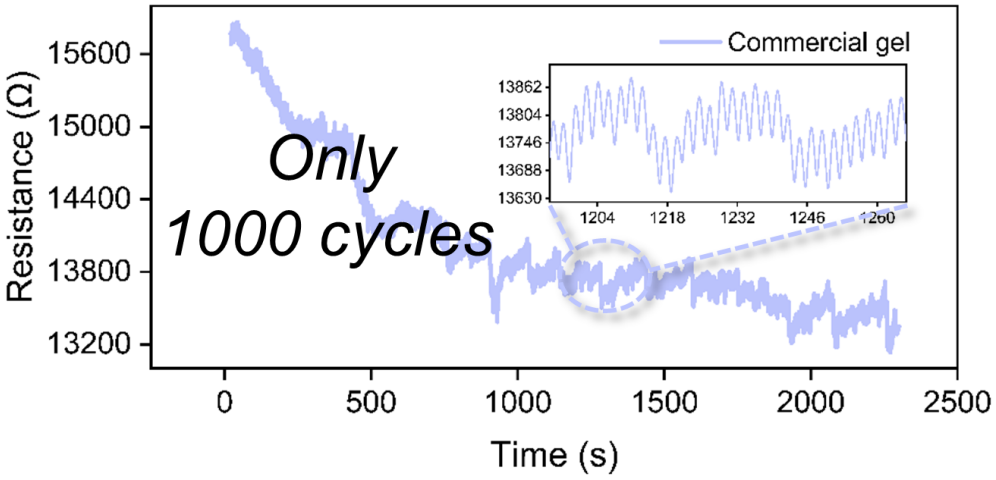

Supplementary Figure 13. The electrical signal response of the commercial gel under 1000 cycles of stretching.

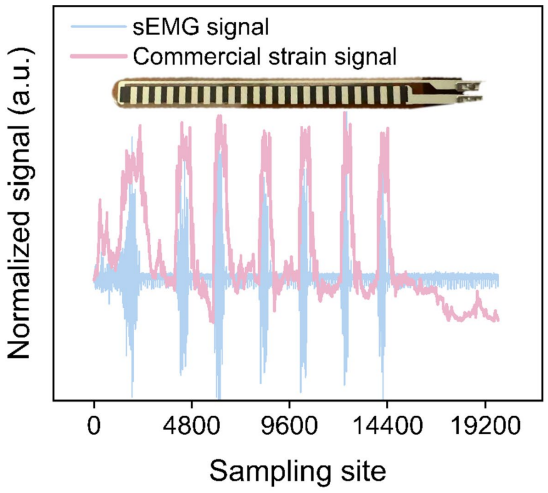

Supplementary Figure 14. Our SEMG sensor, in combination with commercial strain sensors, responds to the signals of flexion and extension of the gastrocnemius muscle area.

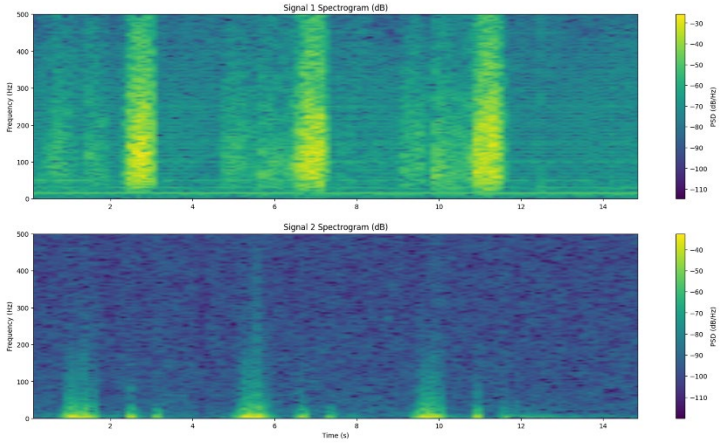

Supplementary Figure 15. Record the frequency domain responses of sEMG and strain signals using Short-Time Fourier Transform (STFT).

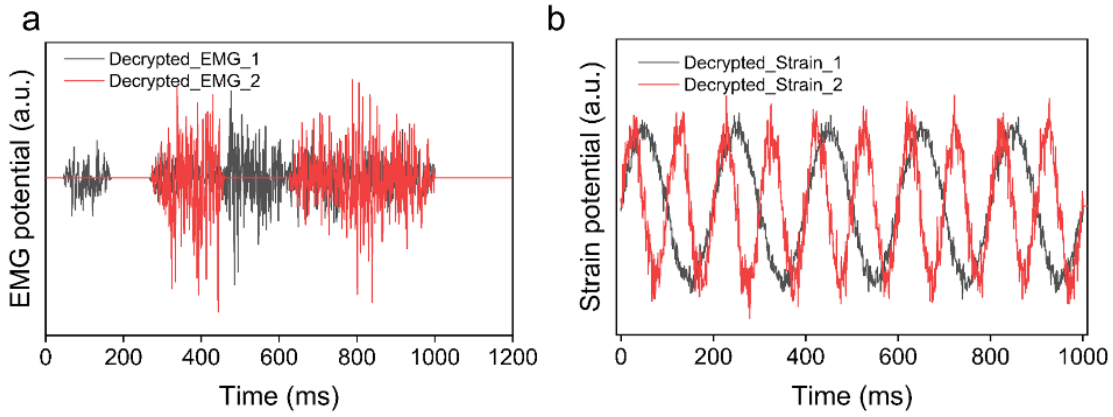

Supplementary Figure 16. Decryption of the a) sEMG and b) strain signals under the known key.

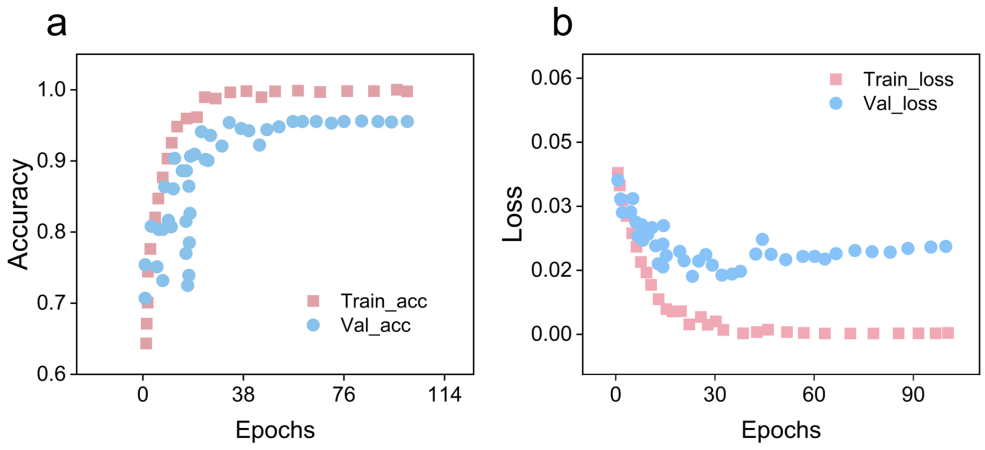

Supplementary Figure 17. Baseline model performance evaluated on plaintext. a) Network training-validation accuracy curves; b) Network training-validation loss curves.

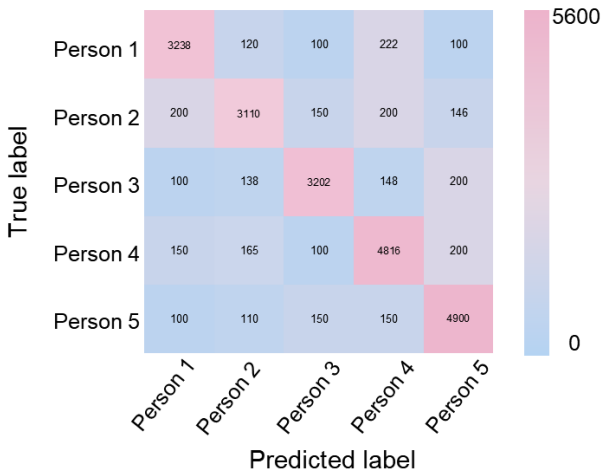

Supplementary Figure 18. Confusion matrix for identity recognition on the 80-day across-session test set.

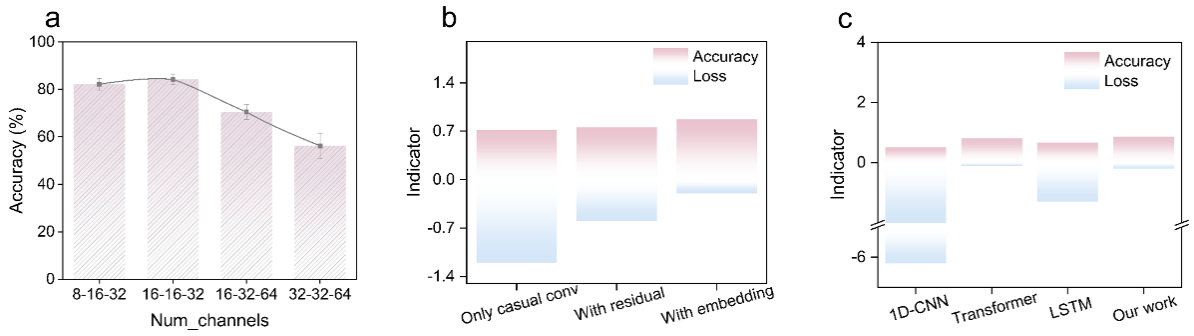

Supplementary Figure 19. a) Parameters of different output channels of the three residual blocks; b) Module ablation experiments; c) Performance comparison of different deep learning models.

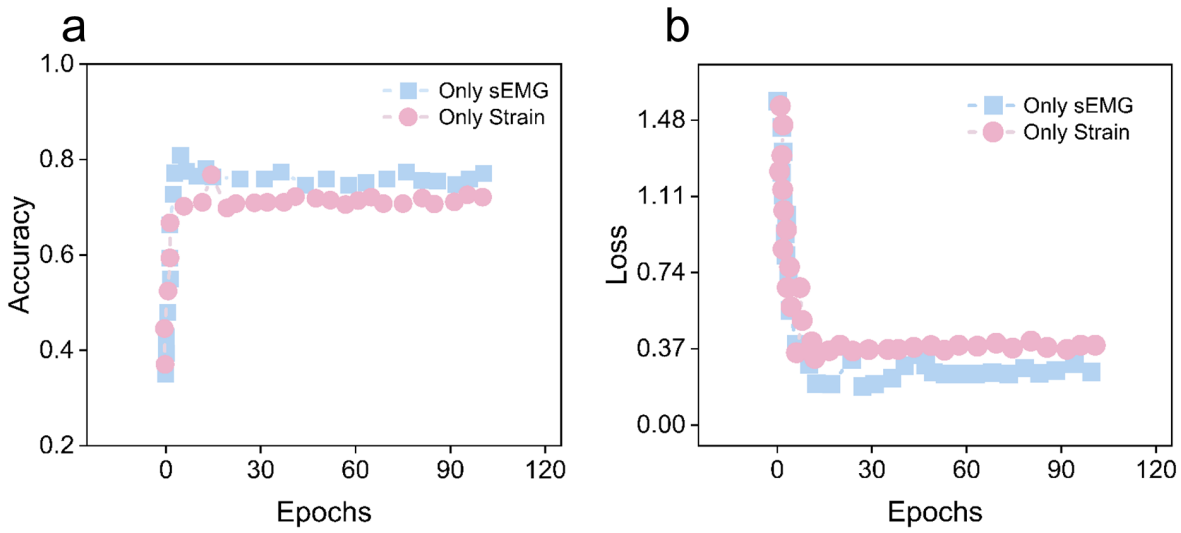

Supplementary Figure 20. Model performance based on single-modal sensing signals. a) Network training-validation accuracy curve; b) Network training-validation loss curve.

Supplementary Table 1. Demographic information of the subjects.

Subject ID	Gender	Age (years)	Height (cm)	Weight (kg)
S01	Male	27	178	76
S02	Male	22	171	70
S03	Female	25	170	62
S04	Male	21	175	72
S05	Female	25	166	60
Mean ± SD	-	24.0 ± 2.4	172.0 ± 4.7	68.0 ± 6.8

Supplementary Table 2. The fracture strength, ductility, and hysteresis ratio of the $PMDU_3$ eutectogel were compared with those of representative low-hysteresis gels reported in the literature, so as to comprehensively evaluate its mechanical properties.

Sample name	Hysteresis rate (%)	Tensile Strength (MPa)	Stretchability (%)
P(HEA-co-AA)[1]	6.4	0.521	1783
P(LA-co-HMA)/[EMIES][2]	8.0	0.420	450
PBA/PEG-BDB[3]	6.0	0.349	1480
P(AM-APBA)[4]	10.0	0.210	1600
P(HEAA-co-BA)/[N4444BF_4][5]	8.0	0.171	578
P(AM-co-AA)/VSNP[6]	7.0	0.131	400
PAA/HPC/EG/$ZnCl_2$[7]	9.0	0.145	210
P(AM-co-THMA)/VBIMBF_4[8]	9.0	0.110	900
PHEA/[C_2MIM][$EtSO_4$][9]	4.5	0.300	850
PVA/TPAL/IL[10]	5.2	0.050	1030
PSBMA/[EMIM][DCA][11]	3.0	0.040	250
EA-PR-[BMIM][TFSI][12]	7.0	0.027	550
PEO/LiTFSI/TEG[13]	16.0	0.200	520
PAM/LSN-Fe[14]	15.0	0.180	1100
P(AN-AM)/OTA/PVDF[15]	13.8	0.150	500
$PMDU_3$ (This work)	1.6	1.364	1023

Supplementary Table 3. Signs of the main cross-peaks in 2DCOS synchronous and asynchronous spectra.

1640	+	-	+	+	+	
1686	-	-	-	+		
1695	-	-	-			
1713	+	-				
1726	+					
1744						
	1744	**1726**	**1713**	**1695**	**1686**	**1640**

Supplementary Table 4. Detailed performance metrics (Precision, Recall, and F1-score) for the 80-day-delayed dataset.

Subject ID	Precision (%)	Recall (%)	F1-score (%)
S01	84.85	88.00	86.40
S02	85.71	84.00	84.85
S03	86.66	87.00	86.83
S04	87.00	86.00	86.50
S05	89.16	87.50	88.32
Average	86.68	86.50	86.58

Supplementary Table 5. Computational complexity comparison.

Model Architecture	Parameters (k)	FLOPs (M)	Accuracy (%)
ByteEmbedded-TCN (Ours)	12.02	4.91	89.7
1D-CNN	9.35	3.70	51.0
LSTM	21.06	8.60	66.3
Transformer	578.82	534.22	81.1

REFERENCES

1. Zheng, Y.; Cui, T.; Wang, J.; et al. Highly stretchable, low-hysteresis, and robust polymeric gels enabled by solvent engineering for wireless sensing and encrypted communication. *Chem. Eng. J.* **2025**, *515*, 163610. DOI: 10.1016/j.cej.2025.163610
2. Liu, S.; Li, Y.; Wen, J.; et al. Versatile Stretchable Conductor with Exceptional Resilience and Rapid Rebound Capabilities: Toward Sustainable and Damage-Resistant Soft Electronics. *Adv. Funct. Mater.* **2024**, *34*, e2313397. DOI: 10.1002/adfm.202313397
3. Wang, Y.; Yu, X.; Zhang, H.; et al. Highly Stretchable, Soft, Low-Hysteresis, and Self-Healable Ionic Conductive Elastomers Enabled by Long, Functional Cross-Linkers. *Macromolecules.* **2022**, *55*, 7845-7855. DOI: 10.1021/acs.macromol.2c00563
4. Xu, K.; Shen, K.; Yu, J.; et al. Ultradurable Noncovalent Cross-Linked Hydrogels with Low Hysteresis and Robust Elasticity for Flexible Electronics. *Chem. Mat.* **2022**, *34*, 3311-3322. DOI: 10.1021/acs.chemmater.2c00093
5. Zhou, C.; Song, X.; Wei, R.; et al. A conductive ionogel with Stretchability, low hysteresis and adjustable adhesion for Air/Underwater mechanosensing. *Chem. Eng. J.* **2024**, *499*, 155992. DOI: 10.1016/j.cej.2024.155992
6. Zhou, J.; Zhao, B.; Liang, Y.; et al. Low hysteresis, water retention, anti-freeze multifunctional hydrogel strain sensor for human-machine interfacing and real-time sign language translation. *Mater. Horizons.* **2024**, *11*, 3856-3866. DOI: 10.1039/d4mh00126e
7. Lu, C.; Wang, X.; Shen, Y.; et al. Skin-Like Transparent, High Resilience, Low Hysteresis, Fatigue-Resistant Cellulose-Based Eutectogel for Self-Powered E-Skin and Human-Machine Interaction. *Adv. Funct. Mater.* **2024**, *34*, e2311502. DOI: 10.1002/adfm.202311502
8. Han, S.; Hu, Y.; Wei, J.; et al. A Semi-Interpenetrating Poly(Ionic Liquid) Network-Driven Low Hysteresis and Transparent Hydrogel as a Self-Powered Multifunctional Sensor. *Adv. Funct. Mater.* **2024**, *34*, e2401607. DOI: 10.1002/adfm.202401607
9. Zhang, L.; Jia, K.; Wang, J.; et al. Stretchable and transparent ionogel-based heaters. *Mater. Horizons.* **2022**, *9*, 1911-1920. DOI: 10.1039/d1mh01775f
10. Cheng, Y.; Zhu, H.; Li, S.; et al. Stretchable, Low-Hysteresis, and Recyclable Ionogel by Ionic Liquid Catalyst and Mixed Ionic Liquid-Induced Phase Separation. *ACS Sustain. Chem. Eng.* **2023**, *11*, 15031-15042. DOI: 10.1021/acssuschemeng.3c03791
11. Sun, Y.; Wang, Y.; Liu, Y.; et al. Biomimetic Chromotropic Photonic-Ionic Skin with Robust Resilience, Adhesion, and Stability. *Adv. Funct. Mater.* **2022**, *32*, e2204467. DOI: 10.1002/adfm.202204467
12. Du, R.; Bao, T.; Zhu, T.; et al. A Low-Hysteresis and Highly Stretchable Ionogel Enabled by Well Dispersed Slidable Cross-Linker for Rapid Human-Machine Interaction. *Adv. Funct. Mater.* **2023**, *33*, e2212888. DOI: 10.1002/adfm.202212888

13. Guo, Y.; Qu, X.; Hu, Z.; et al. Highly elastic and mechanically robust polymer electrolytes with high ionic conductivity and adhesiveness for high-performance lithium metal batteries. *J. Mater. Chem. A.* **2021**, *9*, 13597-13607. DOI: 10.1039/d1ta02579a
14. Zhao, H.; Hao, S.; Fu, Q.; et al. Ultrafast Fabrication of Lignin-Encapsulated Silica Nanoparticles Reinforced Conductive Hydrogels with High Elasticity and Self-Adhesion for Strain Sensors. *Chem. Mat.* **2022**, *34*, 5258-5272. DOI: 10.1021/acs.chemmater.2c00934
15. Luo, R.; Cui, Y.; Li, H.; et al. Fragmented Graphene Aerogel/Polydimethylsiloxane Sponges for Wearable Piezoresistive Pressure Sensors. *ACS Applied Nano Materials.* **2023**, *6*, 7065-7076. DOI: 10.1021/acsanm.3c01285